



Fermi National Accelerator Laboratory

FERMILAB-TM-1815

Effective Length Measurements of Prototype Main Injector Dipole Endpacks

Henry D. Glass, Bruce C. Brown and David J. Harding

*Fermi National Accelerator Laboratory
P.O. Box 500, Batavia, Illinois 60510*

December 1992

Disclaimer

This report was prepared as an account of work sponsored by an agency of the United States Government. Neither the United States Government nor any agency thereof, nor any of their employees, makes any warranty, express or implied, or assumes any legal liability or responsibility for the accuracy, completeness, or usefulness of any information, apparatus, product, or process disclosed, or represents that its use would not infringe privately owned rights. Reference herein to any specific commercial product, process, or service by trade name, trademark, manufacturer, or otherwise, does not necessarily constitute or imply its endorsement, recommendation, or favoring by the United States Government or any agency thereof. The views and opinions of authors expressed herein do not necessarily state or reflect those of the United States Government or any agency thereof.

Effective Length Measurements of Prototype Main Injector Dipole Endpacks

Henry D. Glass Bruce C. Brown
David J. Harding
*Fermi National Accelerator Laboratory**
P.O. Box 500
Batavia, Illinois 60510

March 3, 1993

Abstract

An endpack design has been developed for the Fermilab Main Injector Dipole. A major part of the design process was the testing of a series of prototype removable endpacks. The magnetic parameters that were tested included the effective length and the field shape variation. This report presents a description of the measurement techniques and the results for the effective length. The final endpack has an effective length at 1500 A (0.29T) of 2.6 ± 0.3 mm greater than the steel length, and the change in effective length from 1500 A to maximum current of 9500 A (1.74T) is -1.88 ± 0.05 mm.

1 Introduction

We report measurements of the effective length for a number of endpacks which were mounted on the non-lead end of magnet IDM002, the 2nd prototype dipole for the Main Injector[1]. As of this writing, ten different endpacks have been tested. The last of these endpacks represents the final design, or something very close to it; updated versions of this report may be issued if subsequent endpacks are measured.

*Operated by the Universities Research Association under contract with the U. S. Department of Energy

The endpacks were measured using the 80 inch long (2.032 m) Flatcoil probe. The probe has 24 turns and has a width of 0.268 inches (6.81 mm). The turns were spaced in a geometry which minimizes the sextupole contribution of the flux, as expanded about the probe center. What this means is that although the flux measured by each turn is proportional to the field averaged over the probe area, the total flux, summed over all turns, is very nearly proportional to the field integral along a path running down the geometrical center of the probe. The probe was mounted on a movable stand which allowed us to insert the probe up to 40 inches inside the magnet. In the *baseline* mode of operation, the probe records the difference in flux between zero current and current i :

$$\Delta\Phi(i) = \Phi(i) - \Phi(0).$$

By aligning the long axis of the probe with the longitudinal (z) axis of the magnet, we easily recover the integrated field over the length of the probe:

$$J(z_1, z_2) = \int_{z_1}^{z_2} B(z)dl = \frac{\Delta\Phi}{Nw},$$

where N is the number of turns and w is the probe width; z_1 and z_2 are the endpoint coordinates of the probe. We used a coordinate system where z is zero at the first lamination of the endpack, and is positive going into the magnet. This relation between field integral and flux is correct except for a correction for the remnant field contribution. We have neglected this contribution in our analysis; future plans call for measuring the end field integral by scanning along a path on the z axis with a Hall probe, which is sensitive to the remnant field.

In all of the endpack measurements we position the probe so that z_1 is far outside the magnet, in a region where the field is negligible. One may therefore approximate z_1 as being equal to $-\infty$. The integral then becomes a function solely of the endpoint of the probe that is inside the magnet:

$$J(z) = \int_{-\infty}^z B(z)dl \tag{1}$$

In this case we have assumed that the probe lies along the centerline of the magnet, at $x = 0$. While this is true for all measurements presented here, we will present results in a companion report [2] where we measure the field integral as a function of x .

2 Effective Length Calculation

The total effective length for a magnet excited to a specified current i is

$$\mathcal{L}_{eff}(i) = \frac{\int_{-\infty}^{\infty} B(i, z) dl}{B_0(i)} \quad (2)$$

where B_0 is the mean body field. The total integral may be measured using a probe which extends the entire length of the magnet, and B_0 may be measured by a probe which samples only the body field. In a high quality dipole, the body field is very uniform, only falling off as one approaches close to the ends. With this observation in mind, we can re-express Eq. 2 in terms of the steel length, L_s , and a quantity L_{eff} which we call the *end effective length*:

$$\mathcal{L}_{eff}(i) = L_s + 2L_{eff}(i) \quad (3)$$

The factor of 2 is present because of our definition that L_{eff} is the effective length of each end of the magnet. For simplicity, when we discuss effective length in the remainder of this report, we are referring to L_{eff} . We devised a measurement procedure which measures L_{eff} using the short 80 inch probe. If the probe is inserted a distance z into the magnet, then the quantity

$$\ell(z) = \frac{J(z)}{B_0} - z \quad (4)$$

should become constant and approach L_{eff} as z becomes larger. Experience with this magnet and these endpacks shows this to be true for z between 10 and 20 inches. The body field, B_0 , is determined by performing a linear fit to $J(z)$:

$$J(z) = \alpha + \beta z \quad (5)$$

The slope, β , can be identified as the mean body field in the region $z_{min} < z < z_{max}$ over which the fit is made.

The relative effective length describes the change in L_{eff} with current and can be determined by choosing a reference current, i_0 , and using Equation 4 to obtain

$$\Delta\ell(i, z) = \ell(i, z) - \ell(i_0, z) = \frac{J(i, z)}{B_0(i)} - \frac{J(i_0, z)}{B_0(i_0)} \quad (6)$$

The average of $\Delta\ell(i, z)$ for $z > z_{min}$ is used as the value of $\Delta L_{eff}(i)$. One may see from Equation 6 that this quantity is insensitive to positioning errors in z , a dominant source of systematic errors. For the reference current i_0 we chose 1500 A.

3 Measurement Procedure

We chose a number of z -positions at which to measure $J(i, z)$, moving in 1 inch steps in z for the first 4 inches of the magnet and in 2 inch steps thereafter, up to a maximum z of 20 inches. At each z , we measured the field integral at a number of currents which included 500, 1500, 7000, and 9500 A. For many measurement runs we included a number of additional currents. At each data point we recorded the measurements of the current, the z position, and a quantity, ϕ , equal to the flux divided by the current¹. A VAX was used as the data acquisition computer, which ran the FLATCOIL program [6] to control the measurement process and to record data to disk files. The z position was the only quantity of the measurement process under manual control, both in terms of positioning (via alignment with a steel ruler mounted on the test stand), and recording.

The probe was aligned perpendicular to the face of the laminations. It was centered at $x = 0$, as measured at the endpack edge ($z = 0$). Because of the magnet curvature, this introduced an angle of 0.6° between the probe axis and the magnet axis. The error due to this misalignment increases with z and is dominated by the body field sextupole; at $z = 20$ inches the error at 9500 A is

$$\begin{aligned}\Delta B/B &\approx b_3 x^2 \\ &= b_3 (z \tan \theta)^2 \\ &= (-10 \times 10^{-4}) \times (20 \times \tan(0.6^\circ))^2 \\ &\approx 4.4 \times 10^{-5}\end{aligned}$$

This is smaller than the error due to positioning of the probe in z . We were able to obtain, in typical runs, accuracies between $0.005''$ and $0.010''$. From Equation 5, we estimate that

$$\sigma_J/J \approx \sigma_z/z$$

where we have used the approximation $\beta \approx J/z$. Since σ_z was approximately constant in z , the error in J is worst at low z ; e.g. at $z = 10$ we have $\sigma_J/J \approx 1 \times 10^{-3}$.

¹We recorded ϕ as a first approximation method of correcting for current fluctuations. This method, although inaccurate at higher currents where the magnet saturates, does not adversely affect the measurements described here. A more desirable scheme will be employed at a future date.

4 Endpacks

The endpacks we have measured to date are described in Table 1. The table lists their number and a brief description. References [5] should be consulted for drawings of endpack profiles.

The first two endpacks had a profile in the (y, z) plane which consisted of a single cut at about 66° to the horizontal. The vertex of this cut was located at about -2.5 inches in z . The first endpack was machined to the desired shape out of body laminations. All of the endpacks from #2 on were made using nibbled laminations. Endpack 3 was constructed using a Borda profile [3], which sought to minimize the dependence of effective length on current. This profile was unsuccessful, as measurements presented here show, and Endpack 4 was a modification of #3, in which an additional 1.5" thickness of laminations was bolted on to the exterior of the endpack. An alternate strategy, employing the Rogowsky profile [4], was then used for the succeeding endpacks. Endpack 5, which was machined out of Endpack 2, had an acceptable L_{eff} current dependence, but its absolute effective length was smaller than desired. Some outer laminations were removed from this endpack, and this became Endpack 6, which had an acceptable L_{eff} behavior.

Endpacks beyond #6 were modifications designed to address a secondary requirement, which was to adjust the endpack sextupole to an acceptable value. This topic is addressed in another report [2]. Fortuitously, the efforts at minimizing the sextupole also had the advantage of further reducing the effective length variation.

5 Field Profiles

As a first step in understanding the behavior of the end field, we can calculate the field as a function of z from measurements of $J(z)$. This is simply done by approximating the derivative of J :

$$\overline{B(z)} = \frac{dJ}{dz} \approx \frac{J(z_1) - J(z_2)}{z_1 - z_2},$$

where z is midway between the points z_1 and z_2 at which we have positioned the probe. A useful quantity to examine is the field profile normalized to its value deep inside the body. In Figure 1 we show $B_n = B/B_{body}$ vs z for each of 4 currents for Endpack 9. The region where the profiles for

<i>number</i>	<i>description</i>
1	Machined endpack
2	Nibbled; same profile as 1
3	Borda profile
4	same as 3, with additional 1.5" laminations
5	approximate Rogowsky profile
6	same as 5 but with 9 outer lams removed
7	same as 6 but with noses reduced in size
8	same as 7 with noses further reduced
9	same as 8 with noses gone except for small shims
10	same as 9 with gap between shims widened

Table 1: Endpack descriptions

low and high current are most different occurs where the field begins to drop off, around 2 to 4 inches. This can be seen more readily by plotting $B_{rel}(i, z) = B_n(i, z)/B_n(i_0, z)$, where we choose i_0 to be some suitable low current. In our analysis we chose $i_0 = 1500$ A because its profile was similar to 500 A but had higher signal to noise.

In Figure 2 we plot B_{rel} vs z for 7000 and 9500 A. The minimum in the data at $z = 1.5$ inches presumably corresponds to the point where the relative degree of saturation at high currents is strongest.

Figure 3 shows $B_{rel}(9500A)$ vs z for some representative endpacks. We see that Endpack 9 exhibits the least amount of saturation at the end. As might be expected, the endpacks having a shallow minimum near $z = 2''$ also have a small change of L_{eff} with current.

The profiles are also a useful way of estimating a reasonable value for z_{min} , the lower bound in z for determining a fit to the body field via Equation 5. We have used $z_{min} = 12''$ in our analysis; as justification, we note that, within measurement error, $B_n \approx 1$ for $z > 12''$ for all endpacks.

6 Effective Length Measurements

Using the procedure described in Section 2 we calculated $L_{eff}(i)$ and $\Delta L_{eff}(i)$ for each endpack. The results are listed in Tables 3 through 13. Each table corresponds to a measurement sequence on a given endpack. Some end-

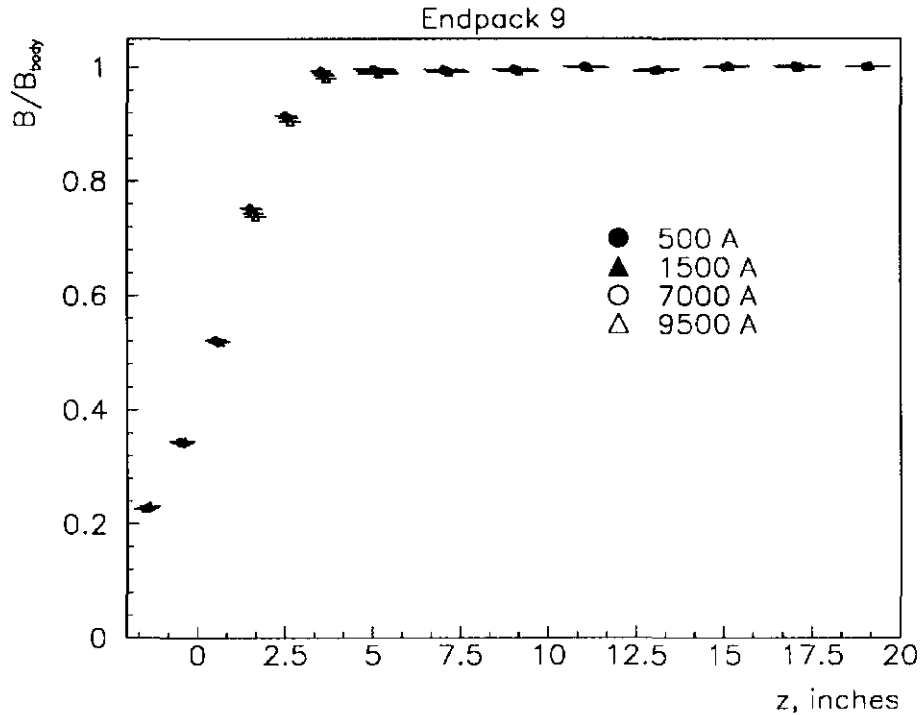


Figure 1: The field profiles, B/B_{body} vs z for Endpack 9 at several different currents.

packs were measured more than once, usually to determine measurement repeatability or to understand the effect of varying some of the measurement conditions. Each row in the tables lists the mean measured current and standard deviation; B_0 , the fitted value of body field divided by the mean current, in units of gauss/ampere; the error in the fit; the value of L_{eff} in mm and its error estimate; and the value of ΔL_{eff} (relative to 1500 A) in mm, and its standard deviation.

Table 2 lists for each endpack measurement a number of ancillary parameters, which include z_{min} , z_{max} , the summary file number, and σ_z (inches). We always used the maximum measured value of z for z_{max} , which was usually 20", except for some early measurements² in which we measured the flux out to 40". The file number references files FCM nnn .002 in direc-

²Endpack 1, file 144; Endpack 2, file 568; and Endpack 4, file 1514

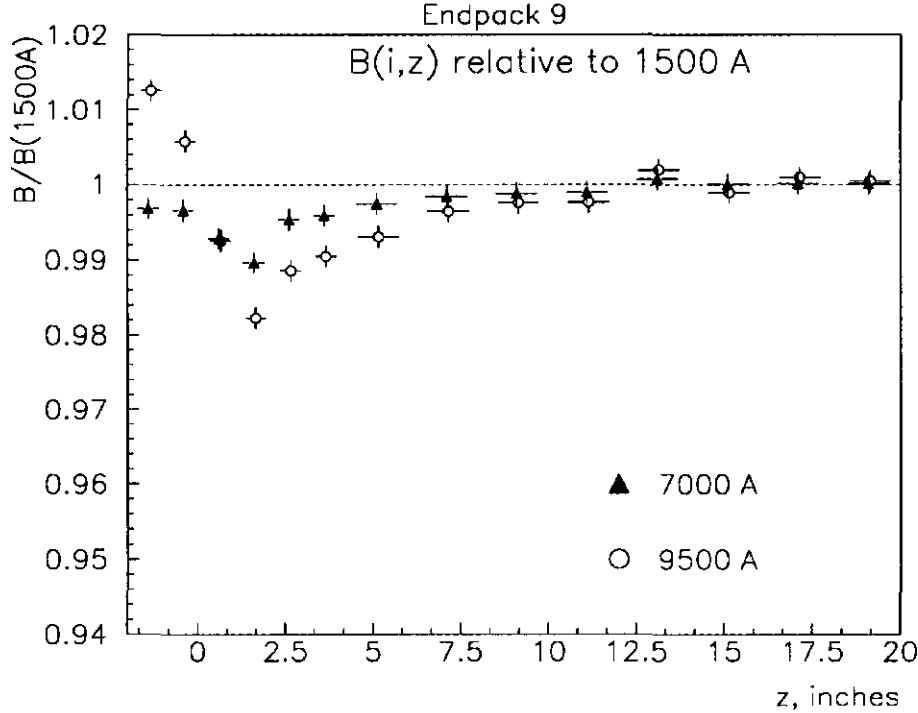


Figure 2: The relative field profiles B_{rel} vs z for Endpack 9 at 7000 and 9500 A.

tory MDTF08::MDTF08\$ROOT:[GLASS.FLATCOIL], which contain summaries of the original flux data. An additional parameter used in the analysis is an estimate of the relative flux error, σ_J/J ; we used a value of 1×10^{-4} throughout our final analysis. This turns out in most cases to be an overestimate (see Section 7) but does not significantly affect the analysis.

Plots of L_{eff} vs current are shown in Figures 4 and 5. A value of zero for L_{eff} means that the effective length is equal to the physical length of the steel; a positive value of L_{eff} means that the effective length is longer than the physical length. Endpacks 9 and 10 had results that were sufficiently similar that only #9 was plotted.

A test of the long-term repeatability of these measurements was done by comparing measurements of Endpack 1 taken one year apart. During this interval, not only had the endpack been removed and subsequently

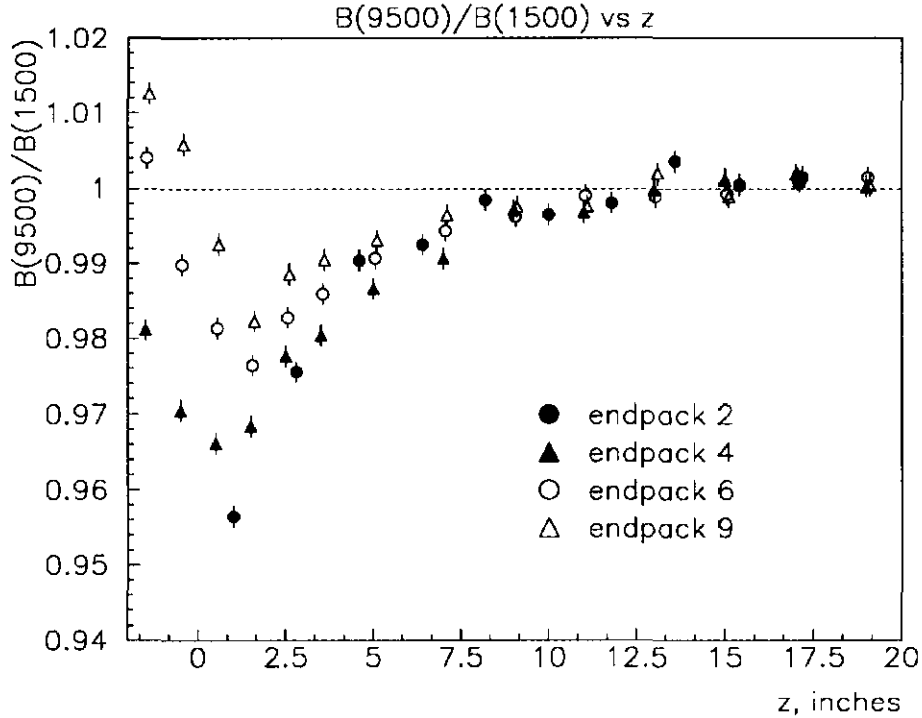


Figure 3: The relative field profile at 9500 Å for selected endpacks.

remounted, but the magnet itself had been removed from the test stand for a period of time. The results are shown in Figure 6. The agreement between the two data sets is very good, except at the lowest currents, where some data acquisition problems were encountered in the earlier data.

7 Error estimates

A set of measurements was taken in order to understand the contribution of z positioning errors to the total error in the flux. First, we took four runs at 1500 Å with the probe fixed at $z = 20''$. These runs produced a standard deviation of the flux equal to $\sigma_{\Phi}/\Phi = 1.6 \times 10^{-5}$. This error was identified as being due to a combination of electronic readout noise and accuracy in magnet current readout. Another four runs were then taken, in which the probe was removed and then repositioned at $z = 20''$ prior to each run. In

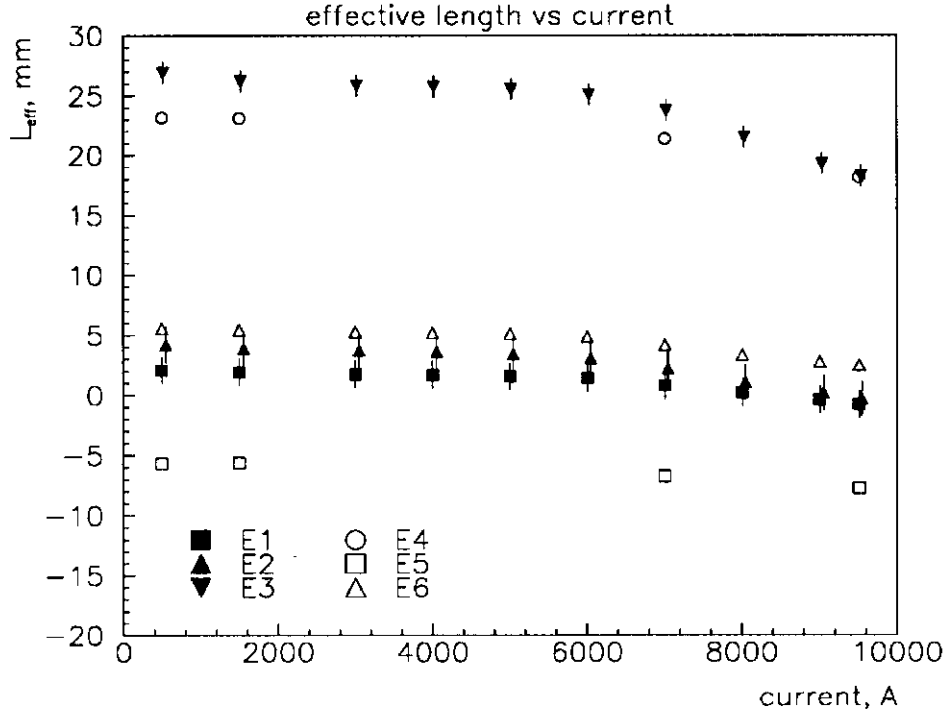


Figure 4: The effective length as a function of magnet current for Endpacks 1-6.

this case we obtained $\sigma_{\Phi}/\Phi = 3.6 \times 10^{-4}$, which we attribute to the combined influence of noise plus z positioning errors. The error due to z positioning alone is estimated from

$$\sigma_{\Phi}^2 = \sigma_{\text{noise}}^2 + \sigma^2(z)$$

This leads to an error in z positioning of $0.007''$. We also repeated these measurements at $z = 10''$ and obtained $\sigma_z = 0.003''$. Averaging these two results gives $0.005''$ (0.13mm), which leads to a systematic error in L_{eff} of 0.37mm (see Eq. 7, below).

The error in the current that we report is the standard deviation for all of the current readings at a particular nominal current setting. This value is typically less than 0.5 A , and is mainly due to the stability of the power supply controller module, power supply noise, and current readout noise. The error in B_0/i is the least squares fitting error in the fit of flux vs z .

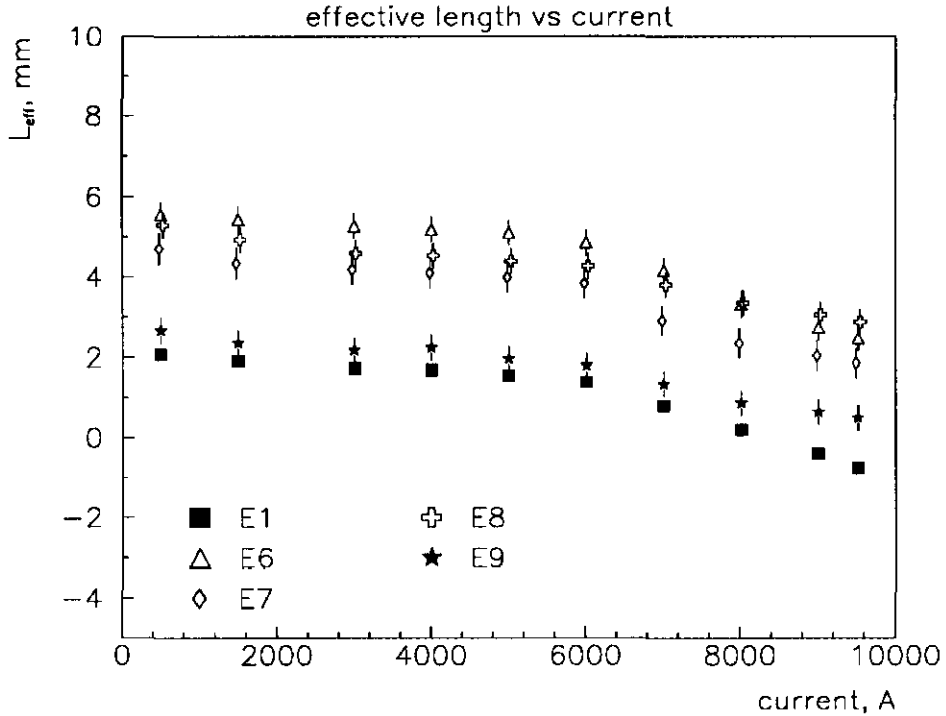


Figure 5: The effective length vs current for Endpacks 6–9, plus Endpack 1 for comparison.

The error reported for L_{eff} is the combined statistical and systematic error. Equation 4 is applied at each data point between z_{min} and z_{max} , and the standard deviation in L_{eff} is used as the statistical error. The systematic error is calculated from

$$\sigma_L^2(sys) = \left[\left(\frac{\sigma_J}{J} \right)^2 + \left(\frac{\sigma_{B_0}}{B_0} \right)^2 \right] \bar{z}^2 + \sigma_z^2 \quad (7)$$

The error in z not only appears explicitly above as the term σ_z but also implicitly, since σ_{B_0} depends strongly on it. In contrast, the errors reported for ΔL_{eff} are only statistical, as the systematic errors are essentially the same between currents.

Plots of the current dependence of ΔL_{eff} are shown in Figures 7 and 8. The overall change in L_{eff} over the entire range of currents decreases

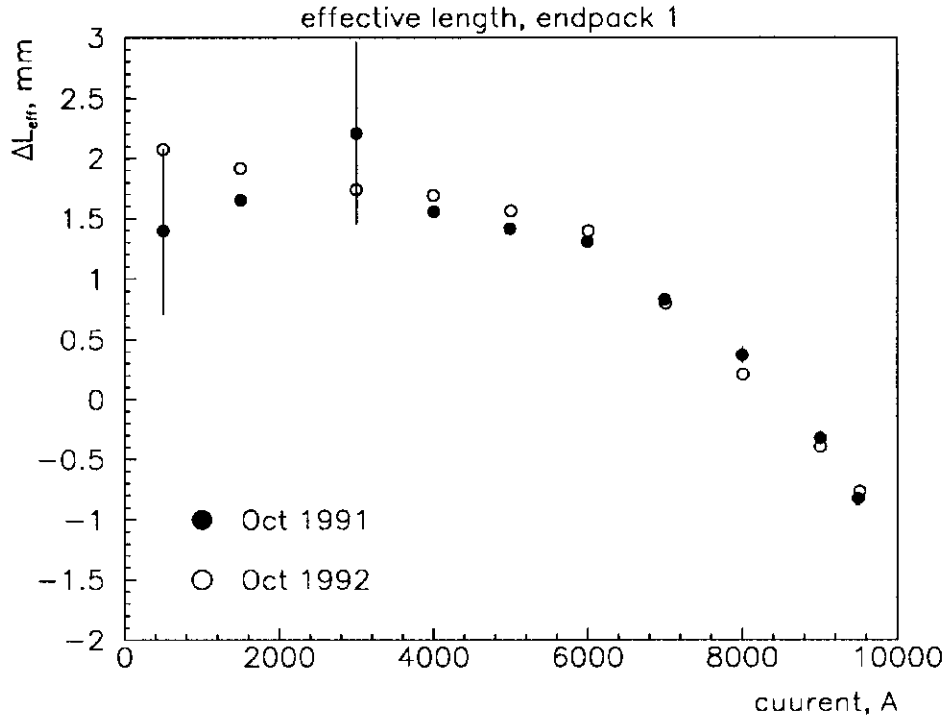


Figure 6: A comparison of the effective length measurements taken on Endpack 1 at two different times.

steadily from Endpacks 6–9, which was the intended effect. (Endpack 10 was sufficiently close to 9 that it was left out of the plot.) The final endpacks meet ΔL_{eff} requirements.

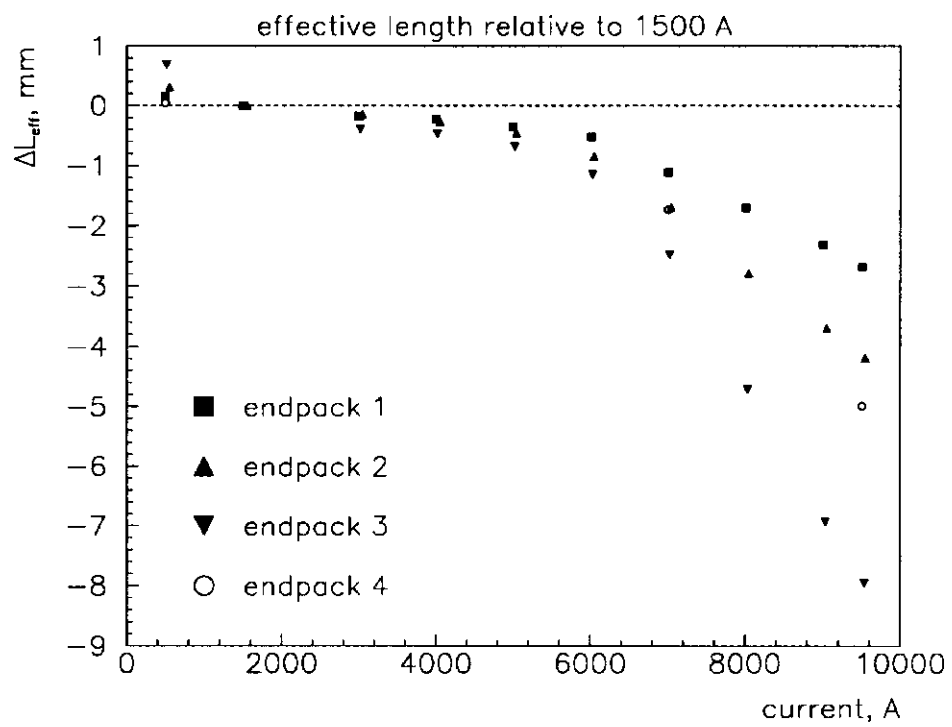


Figure 7: The effective length relative to 1500 A for Endpacks 1-4.

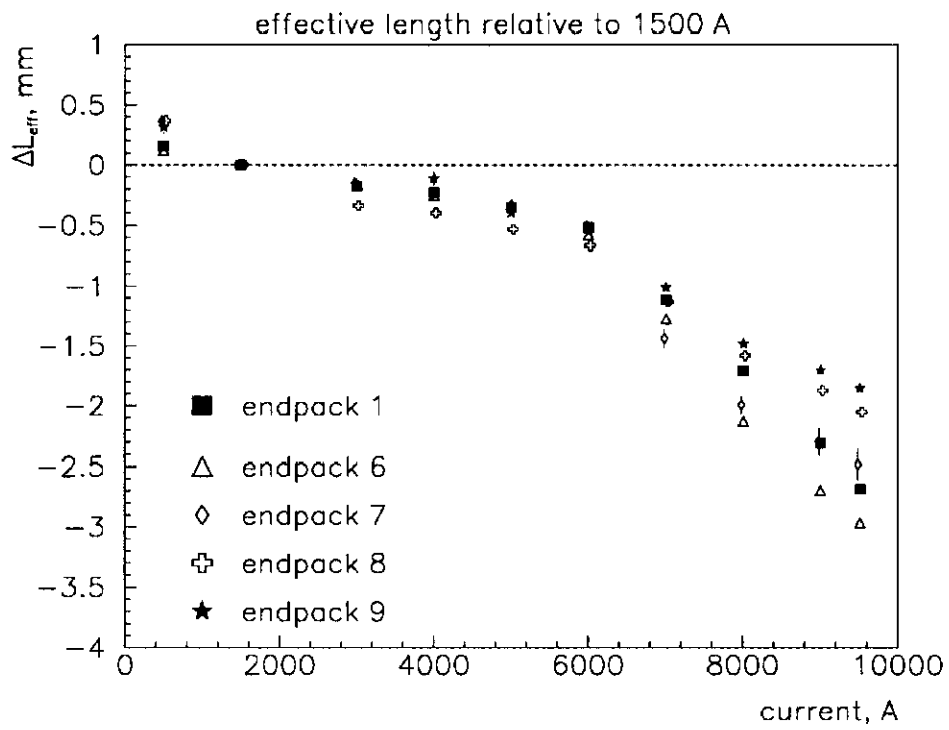


Figure 8: The effective length relative to 1500 A for Endpack 1 and 6–9. The final endpack has the most desirable ΔL_{eff} behavior.

Endpack	file	z_{min}	z_{max}	σ_z
1	144	15.0	39.6	0.010
1	2074	12.0	20.0	0.015
2	568	15.0	40.1	0.030
3	1270	25.0	40.0	0.010
4	1391	12.0	20.0	0.006
5	1530	12.0	20.0	0.004
6	1818	12.0	20.0	0.004
7	1914	12.0	20.0	0.005
8	2147	12.0	20.0	0.004
9	2253	12.0	20.0	0.004
10	2380	12.0	20.0	0.004

Table 2: Auxiliary parameters for endpack data: summary file number, region in z in which fit for B_0 is performed, and estimated z position error.

current, A	B_0/i , gauss/A	L_{eff} , mm	ΔL_{eff} , mm
499.51 ± 0.19	1.93086 ± 0.00100	1.397 ± 0.905	-0.254 ± 0.686
1503.59 ± 0.04	1.94247 ± 0.00101	1.651 ± 0.523	0.000 ± 0.000
2998.89 ± 0.11	1.94234 ± 0.00101	2.207 ± 0.682	0.556 ± 0.751
4003.17 ± 0.22	1.94439 ± 0.00101	1.557 ± 0.536	-0.094 ± 0.047
4992.89 ± 0.11	1.94349 ± 0.00101	1.414 ± 0.526	-0.236 ± 0.039
5998.90 ± 0.20	1.94118 ± 0.00101	1.307 ± 0.523	-0.344 ± 0.034
6998.12 ± 0.14	1.93480 ± 0.00100	0.834 ± 0.517	-0.816 ± 0.032
8000.66 ± 0.29	1.90808 ± 0.00099	0.373 ± 0.516	-1.278 ± 0.066
9006.11 ± 0.20	1.86310 ± 0.00096	-0.322 ± 0.523	-1.972 ± 0.053
9498.39 ± 0.16	1.83639 ± 0.00095	-0.828 ± 0.506	-2.478 ± 0.050

Table 3: Effective length results for Endpack 1 (data file 144)

current, A	B_0/i , gauss/A	L_{eff} , mm	ΔL_{eff} , mm
497.42 ± 0.18	1.93788 ± 0.00465	2.075 ± 1.118	0.158 ± 0.018
1495.69 ± 0.14	1.94948 ± 0.00468	1.916 ± 1.122	0.000 ± 0.000
2998.75 ± 0.12	1.95220 ± 0.00468	1.739 ± 1.124	-0.178 ± 0.015
4002.08 ± 0.25	1.95153 ± 0.00468	1.692 ± 1.123	-0.224 ± 0.013
5006.33 ± 0.36	1.95043 ± 0.00468	1.563 ± 1.122	-0.353 ± 0.012
6008.79 ± 0.52	1.94795 ± 0.00467	1.397 ± 1.120	-0.519 ± 0.010
7011.95 ± 0.28	1.94142 ± 0.00464	0.801 ± 1.120	-1.116 ± 0.011
8010.70 ± 0.44	1.91421 ± 0.00457	0.209 ± 1.122	-1.707 ± 0.038
9009.39 ± 0.56	1.86867 ± 0.00446	-0.393 ± 1.123	-2.310 ± 0.040
9513.94 ± 0.34	1.84056 ± 0.00439	-0.768 ± 1.124	-2.684 ± 0.035

Table 4: Effective length results for Endpack 1 (data file 2074)

current, A	B_0/i , gauss/A	L_{eff} , mm	ΔL_{eff} , mm
499.61 ± 0.20	1.92328 ± 0.00279	4.182 ± 1.480	0.308 ± 0.060
1503.70 ± 0.15	1.93484 ± 0.00280	3.874 ± 1.466	0.000 ± 0.000
2999.14 ± 0.20	1.93727 ± 0.00280	3.724 ± 1.461	-0.150 ± 0.017
4003.52 ± 0.30	1.93678 ± 0.00280	3.607 ± 1.463	-0.266 ± 0.026
4993.46 ± 0.25	1.93564 ± 0.00280	3.416 ± 1.461	-0.458 ± 0.033
5999.27 ± 0.38	1.93338 ± 0.00279	3.031 ± 1.474	-0.843 ± 0.048
6998.69 ± 0.43	1.92669 ± 0.00278	2.179 ± 1.459	-1.695 ± 0.042
8001.31 ± 0.40	1.90054 ± 0.00274	1.085 ± 1.452	-2.789 ± 0.039
9006.85 ± 0.46	1.85558 ± 0.00267	0.174 ± 1.454	-3.700 ± 0.044
9499.32 ± 0.58	1.82866 ± 0.00263	-0.320 ± 1.453	-4.193 ± 0.054

Table 5: Effective length results for Endpack 2

current, A	B_0/i , gauss/A	L_{eff} , mm	ΔL_{eff} , mm
511.63 ± 0.42	1.92883 ± 0.00188	26.919 ± 0.879	0.686 ± 0.014
1514.79 ± 0.37	1.94086 ± 0.00189	26.233 ± 0.881	0.000 ± 0.000
3017.47 ± 0.47	1.94363 ± 0.00189	25.844 ± 0.879	-0.389 ± 0.009
4020.53 ± 0.51	1.94305 ± 0.00189	25.761 ± 0.875	-0.473 ± 0.028
5024.66 ± 0.49	1.94195 ± 0.00189	25.550 ± 0.875	-0.683 ± 0.026
6031.73 ± 0.23	1.93970 ± 0.00189	25.086 ± 0.874	-1.148 ± 0.028
7030.32 ± 0.35	1.93252 ± 0.00188	23.744 ± 0.877	-2.490 ± 0.014
8033.40 ± 0.34	1.90479 ± 0.00184	21.518 ± 0.879	-4.715 ± 0.023
9036.97 ± 0.43	1.85845 ± 0.00179	19.300 ± 0.881	-6.934 ± 0.047
9537.16 ± 0.66	1.83022 ± 0.00177	18.280 ± 0.883	-7.953 ± 0.050

Table 6: Effective length results for Endpack 3

current, A	B_0/i , gauss/A	L_{eff} , mm	ΔL_{eff} , mm
497.15 ± 0.22	1.93361 ± 0.00202	23.166 ± 0.488	0.048 ± 0.025
1495.13 ± 0.08	1.94511 ± 0.00203	23.118 ± 0.480	0.000 ± 0.000
7010.92 ± 0.32	1.93649 ± 0.00201	21.388 ± 0.471	-1.730 ± 0.050
9512.26 ± 0.39	1.83522 ± 0.00189	18.129 ± 0.471	-4.989 ± 0.024

Table 7: Effective length results for Endpack 4

current, A	B_0/i , gauss/A	L_{eff} , mm	ΔL_{eff} , mm
497.19 ± 0.12	1.93506 ± 0.00130	-5.683 ± 0.299	-0.058 ± 0.093
1495.24 ± 0.18	1.94475 ± 0.00131	-5.625 ± 0.314	0.000 ± 0.000
7010.78 ± 0.48	1.93769 ± 0.00130	-6.741 ± 0.299	-1.116 ± 0.086
9512.89 ± 0.44	1.83726 ± 0.00123	-7.749 ± 0.300	-2.124 ± 0.084

Table 8: Effective length results for Endpack 5

current, A	B_0/i , gauss/A	L_{eff} , mm	ΔL_{eff} , mm
497.16 ± 0.08	1.93653 ± 0.00134	5.564 ± 0.315	0.124 ± 0.023
1495.45 ± 0.10	1.94709 ± 0.00135	5.441 ± 0.319	0.000 ± 0.000
2998.24 ± 0.18	1.94943 ± 0.00135	5.275 ± 0.319	-0.166 ± 0.010
4001.51 ± 0.39	1.94889 ± 0.00135	5.186 ± 0.319	-0.255 ± 0.011
5005.58 ± 0.32	1.94744 ± 0.00135	5.107 ± 0.316	-0.333 ± 0.021
6008.26 ± 0.32	1.94518 ± 0.00135	4.858 ± 0.317	-0.582 ± 0.010
7011.02 ± 0.32	1.93848 ± 0.00134	4.164 ± 0.317	-1.276 ± 0.018
8010.05 ± 0.19	1.91133 ± 0.00132	3.312 ± 0.319	-2.129 ± 0.028
9008.54 ± 0.43	1.86459 ± 0.00128	2.743 ± 0.315	-2.698 ± 0.044
9513.56 ± 0.40	1.83580 ± 0.00126	2.474 ± 0.314	-2.967 ± 0.038

Table 9: Effective length results for Endpack 6

current, A	B_0/i , gauss/A	L_{eff} , mm	ΔL_{eff} , mm
497.58 ± 0.24	1.93518 ± 0.00163	4.708 ± 0.393	0.364 ± 0.031
1495.84 ± 0.14	1.94679 ± 0.00164	4.344 ± 0.389	0.000 ± 0.000
2998.78 ± 0.10	1.94907 ± 0.00164	4.193 ± 0.388	-0.152 ± 0.015
4002.25 ± 0.21	1.94857 ± 0.00164	4.104 ± 0.385	-0.241 ± 0.021
5006.41 ± 0.18	1.94734 ± 0.00164	3.996 ± 0.387	-0.348 ± 0.013
6008.93 ± 0.39	1.94495 ± 0.00163	3.838 ± 0.386	-0.507 ± 0.015
7012.08 ± 0.17	1.94025 ± 0.00163	2.907 ± 0.373	-1.438 ± 0.078
8010.80 ± 0.20	1.91304 ± 0.00160	2.350 ± 0.373	-1.994 ± 0.073
9009.56 ± 0.36	1.86607 ± 0.00156	2.046 ± 0.371	-2.298 ± 0.112
9514.37 ± 0.17	1.83738 ± 0.00154	1.862 ± 0.372	-2.482 ± 0.127

Table 10: Effective length results for Endpack 7

current, A	B_0/i , gauss/A	L_{eff} , mm	ΔL_{eff} , mm
497.30 \pm 0.31	1.93358 \pm 0.00134	5.301 \pm 0.313	0.367 \pm 0.031
1495.48 \pm 0.21	1.94506 \pm 0.00135	4.934 \pm 0.312	0.000 \pm 0.000
2998.38 \pm 0.19	1.94825 \pm 0.00135	4.596 \pm 0.311	-0.338 \pm 0.004
4001.88 \pm 0.23	1.94762 \pm 0.00135	4.535 \pm 0.309	-0.399 \pm 0.014
5005.97 \pm 0.30	1.94657 \pm 0.00134	4.399 \pm 0.309	-0.535 \pm 0.013
6008.50 \pm 0.36	1.94410 \pm 0.00134	4.266 \pm 0.309	-0.668 \pm 0.021
7011.75 \pm 0.38	1.93783 \pm 0.00134	3.805 \pm 0.309	-1.129 \pm 0.013
8010.64 \pm 0.46	1.91092 \pm 0.00132	3.352 \pm 0.311	-1.582 \pm 0.010
9009.18 \pm 0.31	1.86450 \pm 0.00128	3.061 \pm 0.308	-1.873 \pm 0.029
9514.25 \pm 0.54	1.83600 \pm 0.00126	2.881 \pm 0.307	-2.053 \pm 0.035

Table 11: Effective length results for Endpack 8

current, A	B_0/i , gauss/A	L_{eff} , mm	ΔL_{eff} , mm
497.00 \pm 0.38	1.93467 \pm 0.00133	2.670 \pm 0.329	0.313 \pm 0.053
1495.21 \pm 0.29	1.94619 \pm 0.00134	2.357 \pm 0.319	0.000 \pm 0.000
2998.13 \pm 0.51	1.94878 \pm 0.00134	2.171 \pm 0.317	-0.186 \pm 0.011
4001.71 \pm 0.48	1.94743 \pm 0.00134	2.244 \pm 0.313	-0.113 \pm 0.053
5005.77 \pm 0.43	1.94722 \pm 0.00134	1.960 \pm 0.315	-0.397 \pm 0.017
6008.46 \pm 0.50	1.94498 \pm 0.00134	1.804 \pm 0.315	-0.553 \pm 0.016
7011.57 \pm 0.52	1.93865 \pm 0.00133	1.347 \pm 0.316	-1.010 \pm 0.010
8010.57 \pm 0.57	1.91225 \pm 0.00131	0.875 \pm 0.318	-1.482 \pm 0.004
9009.18 \pm 0.53	1.86608 \pm 0.00128	0.655 \pm 0.313	-1.702 \pm 0.030
9513.85 \pm 0.29	1.83772 \pm 0.00126	0.504 \pm 0.312	-1.853 \pm 0.031

Table 12: Effective length results for Endpack 9

current, A	B_0/i , gauss/A	L_{eff} , mm	ΔL_{eff} , mm
496.89 ± 0.40	1.93286 ± 0.00133	2.733 ± 0.327	0.095 ± 0.063
1495.14 ± 0.29	1.94337 ± 0.00134	2.638 ± 0.323	0.000 ± 0.000
2998.14 ± 0.17	1.94615 ± 0.00134	2.397 ± 0.320	-0.240 ± 0.012
4001.57 ± 0.28	1.94544 ± 0.00134	2.352 ± 0.322	-0.285 ± 0.034
5005.57 ± 0.37	1.94473 ± 0.00134	2.177 ± 0.317	-0.461 ± 0.061
6008.16 ± 0.37	1.94296 ± 0.00133	1.940 ± 0.317	-0.698 ± 0.030
7011.78 ± 0.26	1.93647 ± 0.00133	1.501 ± 0.312	-1.137 ± 0.088
8010.29 ± 0.30	1.91009 ± 0.00131	1.078 ± 0.316	-1.560 ± 0.058
9008.98 ± 0.36	1.86432 ± 0.00128	0.827 ± 0.310	-1.811 ± 0.054
9513.83 ± 0.51	1.83568 ± 0.00126	0.759 ± 0.312	-1.879 ± 0.054

Table 13: Effective length results for Endpack 10

8 Discussion of Results

These results have converged to an endpack design which meets the requirements for the Main Injector. Let us summarize here the various issues which have been revealed by these studies. Note that the reference for all measurements of z is the outer end of the endpack. Endpack 1 began with a glued stack of laminations which was machined using numerically controlled milling according to the specification provided initially by Stan Snowdon. Endpack 2 was created by modifying the shape of single laminations (nibbling) prior to stacking. This is the technique to be implemented for magnet production and was to be prototyped in this way. It was intended to provide a stepwise approximation to Endpack 1. Endpack 3 was created in the same fashion but with the goal of creating a Borda profile. Endpacks 5–10 were created from Endpack 2 by machining operations. These machining operations were designed, however, to approximate the nibbling which would be done in production.

Looking first at the Borda profile studies using Endpacks 3 and 4, we see that the approximation used for that profile results in a much shorter physical region in z for the transition from body to end. This results in the large positive value of L_{eff} shown in Figure 4. The large change in ΔL_{eff} for Endpack 3 caused us to examine possible sources which might not be easily revealed by the 3-D modeling which was used to predict the

end shape. To examine possible saturation effects near the coil which would be associated with the added flux which extends into the iron-free region, we constructed a 1.5" thick ring of laminations from which the pole portions had been removed. Installing this in the region from $z = -1.5$ to $z = 0$ provided a lower reluctance path for this flux. The improvement of about 30% in the performance suggests that this effect is not negligible. Since this would be an expensive change in the magnet design, and since it did not result in a satisfactory ΔL_{eff} , we did not pursue it. Examination of the L_{eff} results shown in Figure 4 indicates the result that the ΔL_{eff} improvement appears to come from smaller lengths at low field rather than less saturation.

The Rogowsky profile was successively approximated by a single cut (Endpacks 1 and 2) and by a cut plus a series of steps (Endpack 5). Endpack 5 was created from the existing Endpack 2 by modifying the gap at $x = 0$ in a series of steps in z . The resulting profile included laminations for which the iron existed only at distances far from the midplane which reduced L_{eff} without any significant benefit for the field shape or the effective length variation. Following the successful demonstration of the satisfactory effective length variation of the Rogowsky profile approximation of Endpack 5, nine of these laminations were removed and additional body laminations added to maintain the steel length. The measurements indicate that about 11 mm were added to the effective length of the end from adding about 13.5 mm of body laminations. In addition, examination of the profile in the $y - z$ plane reveals that Endpack 6 is a better approximation to the Rogowsky profile. Modifications to create Endpacks 7-10 involved only modifications of the laminations at $x \neq 0$, which were designed to produce improvements in the transverse field behavior. They also improved the ΔL_{eff} behavior.

We can expect small changes when implementing this design in production magnets. The matching of bolted endpack halves to each other and to the body was much less perfect than will be the case in production. In particular, the spring created by the lamination stack must be overcome at the end by a net bowing of the end laminations. This bowing makes it difficult to match to the stacked end of the magnet but the net displacements will have negligible effect of the final shape of the field. Endpacks were mounted with the constraint of minimizing the gap errors on the top-to-bottom parting plane (reduced to less than 0.005") which left larger gaps for some assemblies between the endpack and the body steel. Additional small endpack design changes will be implemented to improve coil clearances. Endpack 11 will be constructed with laminations of this iterated design to confirm these small changes.

9 Acknowledgments

The authors thank Dave Hartness, Shree Agrawal, and Mark Thompson for their excellent work in performing the measurement activities on these endpacks. We also thank Steve Helis for his efforts on construction of the probe. Additional assistance was provided by Butch Bianchi, Jim Garvey, Harold Stahl, and Peter Mazur.

References

- [1] Pertinent details regarding the Main Injector Dipole may be found in the Conceptual Design Report for the Fermilab Main Injector, Rev. 2.3, April 1990.
- [2] H. Glass et. al., "Field Shape Measurements of Main Injector Dipole Endpacks," MTF-92-019.
- [3] F. Ostiguy, private communication.
- [4] F. Ostiguy, private communication.
- [5] D. Harding et. al., "Design and Measurements of Prototype Main Injector Dipole Endpacks," (in preparation), to be presented at 1993 Particle Accelerator Conference, Washington, DC.
- [6] At present, on-line documentation describing the FLATCOIL data acquisition program can be found in the MSR\$ROOT:[DOC] directory on node MDTF00::.